

PAPER • OPEN ACCESS

A two-phase Hessian approach improves the DFT relaxation of slabs

To cite this article: P A G Davies and W M C Foulkes 2018 *J. Phys.: Condens. Matter* **30** 315901

View the [article online](#) for updates and enhancements.



IOP | ebooks™

Bringing you innovative digital publishing with leading voices to create your essential collection of books in STEM research.

Start exploring the collection - download the first chapter of every title for free.

A two-phase Hessian approach improves the DFT relaxation of slabs

P A G Davies[✉] and W M C Foulkes[✉]

Department of Physics, Imperial College, Prince Consort Road, London SW7 2AZ, United Kingdom

E-mail: p.davies10@imperial.ac.uk

Received 27 February 2018, revised 31 May 2018

Accepted for publication 19 June 2018


Published 6 July 2018



Abstract

A two-phase Hessian approach to DFT slab relaxation of slabs has been implemented and tested. It addresses weaknesses in the modified Broyden and Pfrommer BFGS algorithms specific to relaxing slabs. Complete Hessian and then inverse Hessian matrices with no strain/stress components are first constructed at high force signal-to-noise ratios with no accompanying relaxation. In a second phase the static inverse Hessian is used to relax the slab down to a low force tolerance.

Keywords: condensed matter theory, density functional theory, slab relaxation, BFGS, Broyden, computational methods

 Supplementary material for this article is available [online](#)

(Some figures may appear in colour only in the online journal)

1. Introduction

DFT calculations are often used to find the equilibrium conformations of groups of atoms: the forces on the atoms are calculated using DFT and the atoms moved until those forces are within a defined tolerance of zero. Some investigations into ferroelectricity in slabs need precise phonon and polarisation calculations based on residual atomic forces in the range of 10^{-4} – 10^{-5} eV Å⁻¹ [4, 8, 10, 14], which are difficult to attain. This applies particularly to thicker slabs and lower phonon frequencies. Other applications can have similar requirements.


When performing DFT simulations of SrTiO₃, there was a requirement to distinguish between relative permittivities of 300 and 500, at an applied external electric field of 1 V Å⁻¹, equivalent to an approximate polarisation of 0.1 C m⁻². This requires a polarisation resolution of around 1.3×10^{-4} C m⁻². Calculations using a B-site cation Born dynamic charge of 8 [16], LDA (local density approximation exchange correlation

functional) value for the bulk modulus of 220 GPa [12] and lattice constant of 4 Å give a nominal maximum force on any one atom of 3.4×10^{-4} eV Å⁻¹. However, the SrTiO₃ polarisation is mainly dependent on the Ti ion movement, which forms part of the ‘soft-mode’ transverse optical phonon, for which the spring constant will be significantly less than indicated by the bulk modulus. Hence our force tolerance convergence target was set to 10^{-4} eV Å⁻¹.

This paper concerns the problems encountered when attempting to use conventional DFT-based approaches to relax the atomic positions of slabs with more than a few layers to very low force tolerances.

The modified Broyden quasi-Newton algorithm as described in Johnson 1988 [5] and the BFGS (Broyden–Fletcher–Goldfarb–Shanno) quasi-Newton algorithm as modified and described by Pfrommer *et al* 1997 [11], while good at relaxing bulk solids, do not work well for perovskite slabs more than 8 unit cells thick in a vacuum. These algorithms are described in detail in books such as Numerical Recipes by Press *et al* [13] and Numerical Optimization by Nocedal and Wright [9].

Figure 1 shows the BFGS relaxation of a layered slab with a first layer of 3 unit cells thickness of SrTiO₃, a second layer of 6 unit cells thickness of SrRuO₃ and a final layer of 3 unit

 Original content from this work may be used under the terms of the [Creative Commons Attribution 3.0 licence](#). Any further distribution of this work must maintain attribution to the author(s) and the title of the work, journal citation and DOI.

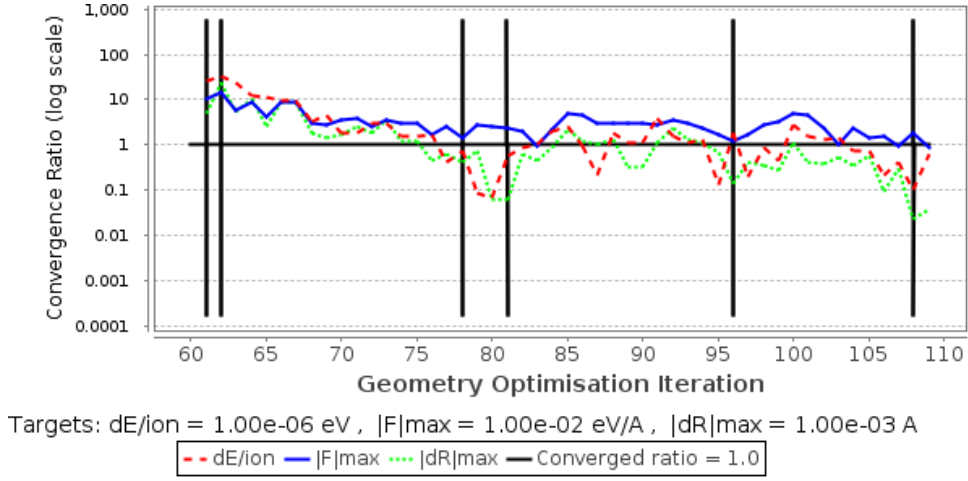


Figure 1. This charts the convergence of iterations of BFGS geometry relaxation across multiple CASTEP DFT runs for a slab with layers of $SrTiO_3 \times 3$ unit cells, $SrRuO_3 \times 6$ unit cells and $SrTiO_3 \times 3$ unit cells normal to the slab surface and surrounded by vacuum. The DFT SCF (self-consistent field) step electronic energy convergence was set to 10^{-7} eV per atom. Three measures of convergence are shown. $|F|max$ (blue, continuous line) is the maximum residual force on any atom as a ratio of the target. dE/ion (red, dashed) is the change in total energy per iteration, averaged per atom, and $|dR|max$ (green, dotted) is the largest atom move between iterations, both as ratios of their respective targets. Vertical black lines denote the start of new relaxation runs. From iteration 78 onwards the residual forces are almost random just above 10^{-2} eV Å $^{-1}$ (force convergence ratio of 1) with no obvious downward trend. There appears to be little chance of getting down to 10^{-4} eV Å $^{-1}$ (force convergence ratio 10^{-2}).

cells thickness of $SrTiO_3$. The entire slab is surrounded by vacuum at both surfaces. The DFT electronic energy convergence was set to 10^{-7} eV per atom. $|F|max$, the blue continuous line, is the maximum absolute residual force on any atom as a ratio of the convergence target of 0.01 eV Å $^{-1}$. Hence a convergence ratio of 3 would represent a maximum atomic force of 3×10^{-2} eV Å $^{-1}$. Vertical black lines denote the start of new relaxation runs.

The maximum residual atomic force convergence ratio shows a downward trend from iterations 61–78, and thereafter oscillates randomly between 8 and 1 (representing 8×10^{-2} to 1×10^{-2} eV Å $^{-1}$). All three parameter ratios reduce to below their respective convergence ratios of 1 at iteration 108. Meeting the convergence criterion appears to be more a matter of random chance than a consistent downward trend. There seems little chance of getting down to 10^{-4} eV Å $^{-1}$ (force convergence ratio 10^{-2}).

Our project required DFT relaxation of perovskite slabs of 12 and 14 unit cells in a vacuum down to atomic forces of less than 10^{-4} eV Å $^{-1}$. Without manual intervention such low tolerances could not be obtained using standard DFT codes such as CASTEP (Cambridge Serial Total Energy Program) described in Clark *et al* 2005 [3], a plane-wave DFT code, or SIESTA (Spanish Initiative for Electronic Simulations with Thousands of Atoms) [1], an atomic-like orbital DFT code. CASTEP implements the standard DFT version of the Pfrommer BFGS algorithm. SIESTA uses the modified Broyden algorithm.

Inspection of the forces during slab relaxations indicated that a manual approach might succeed where the standard algorithms failed. After the successful manual relaxation of a simple slab, an automated algorithm more suited to slabs was defined and implemented. That is described here.

$$\Delta \mathbf{F} = \begin{pmatrix} \Delta \sigma_1 \\ \Delta \sigma_2 \\ \vdots \\ \Delta \sigma_8 \\ \Delta \sigma_9 \\ \Delta F_{10} \\ \Delta F_{11} \\ \vdots \\ \Delta F_{3N+8} \\ \Delta F_{3N+9} \end{pmatrix}, \Delta \mathbf{X} = \begin{pmatrix} \Delta \epsilon_1 \\ \Delta \epsilon_2 \\ \vdots \\ \Delta \epsilon_8 \\ \Delta \epsilon_9 \\ \Delta X_{10} \\ \Delta X_{11} \\ \vdots \\ \Delta X_{3N+8} \\ \Delta X_{3N+9} \end{pmatrix}.$$

Figure 2. Change vector structures for strain/individual atomic displacements and stress/atomic forces. In this notation $\Delta \sigma_1 = \Delta \sigma_{11}$, $\Delta \sigma_2 = \Delta \sigma_{12}$ and $\Delta \sigma_9 = \Delta \sigma_{33}$ etc.

2. Pfrommer BFGS approach

2.1. Pfrommer BFGS relaxation

In the linear regime the Pfrommer BFGS relaxation process for N atoms with $3N$ independent co-ordinates defines a Hessian matrix A as follows :

$$\Delta \mathbf{F} = A \Delta \mathbf{X} \quad (1)$$

where $\Delta \mathbf{F}$ is the set of stress tensor $\Delta \sigma_i$ and atomic force ΔF_i component changes and $\Delta \mathbf{X}$ is the set of strain tensor changes $\Delta \epsilon_i$ and atomic fractional coordinate changes ΔX_i as in figure 2.

$$H = \left(\begin{array}{ccc|ccc} C_{11} & \dots & C_{19} & X_{110} & \dots & X_{13N+9} \\ \vdots & \ddots & \vdots & \vdots & \ddots & \vdots \\ C_{91} & \dots & C_{99} & X_{910} & \dots & X_{93N+9} \\ \hline X_{101} & \dots & X_{109} & H_{1010} & \dots & H_{103N+9} \\ \vdots & \ddots & \vdots & \vdots & \ddots & \vdots \\ X_{3N+91} & \dots & X_{3N+99} & H_{3N+910} & \dots & H_{3N+93N+9} \end{array} \right)$$

Figure 3. Structure of the inverse Hessian relaxation matrix.

If the Hessian matrix A is known, it can be inverted to give a negative semidefinite inverse Hessian matrix H such that

$$\Delta \mathbf{X} = A^{-1} \Delta \mathbf{F} = H \Delta \mathbf{F} \quad (2)$$

which drives the relaxation process.

Care must be exercised during the inversion. The matrix A can be decomposed into eigenvalues λ^k and eigenvectors \mathbf{e}^k , and the inverse matrix would normally then be specified as

$$H_{ij} = \sum_k \frac{\mathbf{e}_i^k \mathbf{e}_j^k}{\lambda^k}. \quad (3)$$

For a 3D bulk relaxation, up to six orthogonal eigenvectors of A form the basis set for translations and rotations of the entire structure. In an exact representation of A , the translations have eigenvalues of zero, as the force between atoms does not change on displacing the whole structure. Periodic boundary conditions on the DFT supercell will normally prevent rotations from having zero eigenvalues. The corresponding $\mathbf{e}_i^k \mathbf{e}_j^k / \lambda^k$ terms with zero eigenvalues must be omitted from the summation in (3).

Consider the effect of an set of ion displacements $d\mathbf{e}^i$ which are a multiple d of the i^{th} non-zero eigenvector \mathbf{e}^i of A . If the atoms are perturbed from an equilibrium position then the restoring force must be in exactly the opposite direction. Hence all the non-zero eigenvalues of H must be negative. Both A and H must therefore be negative semidefinite matrices.

The stress tensor σ is defined in terms of the individual strain tensor components ϵ_{ij} by

$$\sigma_{ij} = \frac{1}{\Omega} \frac{\partial U}{\partial \epsilon_{ij}} \quad (4)$$

where U is the energy and Ω the supercell volume as in Knuth *et al* 2015 [7]

2.2. Structure of the inverse Hessian relaxation matrix

The block structure of the Pfrommer BFGS inverse Hessian relaxation matrix is illustrated in figure 3. The top left block maps stress to changes in strain tensor components. The bottom right block maps atomic forces to changes in individual ion fractional coordinates.

In normal bulk solids, where all bonds are of somewhat similar strength, the upper right X_{ij} cross terms mapping atomic forces to strain changes, and lower left X_{ij} cross terms mapping stress to atomic displacements would typically be small, but may not necessarily be zero. But if a previously relaxed

material has a plane of atoms with weak bonding on one side and strong bonding on the other, a uniform stretch normal to the plane creates non-zero net atomic forces on some atoms in the plane, which would introduce significant upper right and lower left X_{ij} cross terms in the inverse Hessian.

Pfrommer *et al* 1997 [11] recommend a specific block-diagonal, initial inverse Hessian matrix which has 9 identical scalar terms on the top left diagonal relating strain and stress, and 3×3 blocks on the bottom right diagonal relating atomic forces to changes in position.

Starting with this initial inverse Hessian, the $n + 1^{\text{th}}$ move is calculated using the Pfrommer *et al* 1997 [11] formulae

$$\Delta \mathbf{X}_n = H_n \mathbf{F}_n \quad (5)$$

$$\mathbf{X}_{n+1} = \mathbf{X}_n + \lambda \Delta \mathbf{X}_n \quad (6)$$

where λ is determined by a line minimisation. Close to equilibrium, $\lambda = 1$ is the only value used most of the time.

After each step, the new values for the atomic forces are calculated and the inverse Hessian is modified using a formula given in Pfrommer *et al* 1997 [11].

In theory, in the harmonic regime, for a system of N independent atoms, after $3N$ moves the inverse Hessian should be fully developed and the structure fully relaxed.

2.3. Weaknesses of the Pfrommer BFGS approach applied to slabs

For both slab and bulk solid relaxations, the inverse Hessian matrix H must remain negative semidefinite. That is, if \mathbf{v} is any non-zero vector then the scalar

$$s = \mathbf{v}^* H \mathbf{v} \quad (7)$$

must be either zero or a negative real number.

For noise-free forces, and displacements from equilibrium in the quadratic regime, H can be shown to be negative semidefinite by representing \mathbf{v} in terms of the orthogonal eigenvectors \mathbf{e}^m of A and H as follows :

$$\mathbf{v} = \sum_m C^m \mathbf{e}^m. \quad (8)$$

From (3), using the fact that the eigenvectors \mathbf{e}^m are orthogonal:

$$\begin{aligned} \mathbf{v}^* H \mathbf{v} &= \sum_m (C^m)^* \left(\frac{1}{\lambda^m} \right) C^m \\ &= \sum_m \frac{(C^m)^* C^m}{\lambda^m}. \end{aligned} \quad (9)$$

$(C^m)^* C^m$ is always positive. From section 2.1 Pfrommer BFGS relaxation, all the eigenvalues λ^m of A are negative or zero. The eigenvectors corresponding to zero eigenvalues of A are not used in the construction of H . Thus for any \mathbf{v} , which is a linear combination solely of such excluded eigenvectors, the effective eigenvalue of H is zero. Hence

$$\mathbf{v}^* H \mathbf{v} \leq 0 \quad (10)$$

and H is therefore negative semidefinite.

After each move, CASTEP performs an indirect check that H is still negative semidefinite. Although detailed checking

confirmed that CASTEP accurately implements the Pfrommer BFGS algorithm, for the slabs of interest, the check that H was negative semidefinite failed every 4 or 5 moves. This resulted in a reset of H to its initial values. Working closely with members of the CASTEP development team did not enable them to identify a potential fix for the problem. Although the exact cause of the failure to stay negative semidefinite is unknown, it may be related to noise in the forces. It is relevant to some of the problems in relaxing slabs discussed below.

One specific difference between relaxations of slabs and bulk systems is the presence of a null move. This consists of a change in strain normal to the slab, exactly counterbalanced by changes to atomic fractional coordinates in the same direction. Although both changes are non-zero, there is no change to the relative position of bonded atoms, measured in Ångströms (although the size of the DFT supercell vacuum region is no longer the same). The corresponding eigenmode has an eigenvalue of zero. If this is not removed during incremental updating of the inverse Hessian it can potentially cause numerical problems as the corresponding inverse Hessian eigenvalue diverges.

Another problem arises because average strain in a slab is directly caused by the movements of surface atoms, and not those in the interior of the slab.

For a bulk solid at equilibrium, the forces on each atom are zero. Applying a small tensile strain, in the direction of one unit cell lattice vector, will produce a proportionate stress. If the bulk solid consists of only one type of atom, this should produce no net atomic forces. If the bulk solid consists of multiple atomic types, and all bonds are of similar strength, it will produce only small net atomic forces, as forces from stretched bonds in one direction will mainly be offset by forces from stretched bonds in the opposite direction. However, the stress and crystal energy will increase as the crystal is stretched relative to the lowest energy equilibrium configuration. Application of the initial inverse Hessian to the stress tensor of the strained material defines a change in strain approximately equal and opposite to the original strain applied, leaving small local atomic forces to be relaxed away.

A slab at equilibrium does not behave the same way. A small tensile strain normal to the slab surface will not only cause a proportionate stress, but also a net force towards the slab centre on atoms at the slab surface. These atoms have no outward-facing bonds to counterbalance the inward force due to the stretched inside bonds. The multiplication of the stress and atomic force vector by the initial inverse Hessian will define, not only a recommended strain change, but also superfluous fractional coordinate moves to slab surface atoms. In the next iteration, the forces on the atoms in a plane are transmitted, diluted, to the next inward atomic plane, and so on. In theory the dynamic updates to the inverse Hessian will eventually introduce cross terms between stress and atomic moves in fractional coordinates, and between surface atom atomic forces and strain. Although these should lead to an effective inverse Hessian for the slab, this did not happen, prevented by resets of the inverse Hessian, which was no longer negative semidefinite after each four or five relaxation iterations, as discussed above.

Suppressing changes to supercell lattice constants to switch off the processing of stress and strain also fails. Strain-like distortions of the whole slab, would be present, for example, if the lattice parameter normal to the surface were incorrect. These must then be relaxed by motions of individual atoms, related to the atomic forces via the lower right-hand block of the inverse Hessian matrix. Unfortunately, the only large net atomic forces present in a strained slab are those on the surface layers; the bonds inside the slab are stretched too, but bulk atoms have similar forces in opposite directions which mainly offset each other to leave a much smaller net force. To correct the larger forces on only the surface atoms requires correlated moves of at least $(N - 1)/2$ atoms before the BFGS inverse Hessian is fully developed. When there is significant noise in the DFT forces, to develop such a correlated move from the initial inverse Hessian is difficult. The relaxation of a stretched slab produces waves of atomic moves towards the centre, decaying as they propagate.

As the relaxation proceeds, and the atomic forces reduce, the finer-resolution updates to the inverse Hessian matrix take place at decreasing force signal-to-noise ratios, also making optimum convergence less likely.

A slab can be viewed as a system for which, applying the usual DFT periodic boundary conditions, the bond via the vacuum between the two slab surfaces is just extremely weak. Other systems contain both weak and strong bonds, such as an array of molecules bonded together by Van der Waals forces. Therefore, for these systems, similar problems are expected to arise and the standard Pfrommer BFGS algorithm may not be effective.

3. Modified Broyden relaxation

Johnson 1988 [5] developed a modified version of the Broyden 1965, quasi-Newton minimisation method [2] for coupled systems of non-linear equations. This combined Srivastava's 1984 [17] modifications to the Broyden method, which minimised use of memory, with Vanderbilt and Louie's 1984 [18] process and convergence improvements. Although emphasising the application of the modified Broyden method to electronic-structure energy minimisation, Johnson notes that it can also be used for molecular-dynamics simulations.

Johnson defines the modified Broyden algorithm using a Jacobian matrix, whereas Pfrommer [11] defines enhancements to BFGS using a Hessian. However, a Hessian is the Jacobian of a gradient, and the Jacobian of a force vector is equivalent to the Hessian of an energy scalar, so, while differing in detail, the two methods are based on similar constructs.

The reasons why modified Broyden relaxation failed for our slabs were not investigated in detail. However, due to the similarities between the methods, the reasons for failure of modified Broyden to relax thick slabs sufficiently are likely to be similar to those causing Pfrommer BFGS to fail. Both the presence of a null move, causing divergence, and the interference of surface atom forces and positions with standard stress and strain processing, are likely to contribute to the failure to

relax slabs sufficiently, as described in section 2.3 *Weaknesses of the Pfrommer BFGS approach applied to slabs*.

4. The two-phase Hessian approach

A more robust approach to high precision relaxation of a slab in a vacuum is to completely determine the inverse Hessian matrix at a relatively large force signal-to-noise ratio before using it to drive the relaxation of the structure in a second, separate phase. The better force signal-to-noise ratio results in a more accurate inverse Hessian than one built dynamically during relaxation, allowing convergence to a lower force tolerance.

The stress/strain mapping is dropped from the inverse Hessian. In its place, the algorithm relies on sufficient precision in the formation of the Hessian matrix to identify relaxation modes involving moves of most of the atoms in the structure. This enables the algorithm to respond to stresses induced by a pure strain without incorporating an explicit strain/stress mapping. Hence the process uses a fixed supercell lattice vector in the direction normal to the slab surface. This approach is suitable only for slabs and not for bulk materials, for which the stress/strain processing is relatively independent of that for atomic forces and fractional coordinate positions.

An effective two-phase automatic method of performing 1D relaxations in the direction perpendicular to the surface of the slab is as follows:

Phase 1—Hessian discovery and processing

1. A DFT run is performed for a base configuration with fractional coordinates \mathbf{X}^{base} , producing forces \mathbf{F}^{base} . For the i^{th} independent atomic coordinate the positions and forces are X_i^{base} and F_i^{base} . Each atomic coordinate specifies the position along the axis normal to the slab of one atom or a set of atoms constrained to the same coordinate.
2. A series of DFT runs is performed, equal in number to N , the number of independent atomic coordinates, during each of which only a single independent coordinate is temporarily displaced from the base atomic coordinates by a displacement h , chosen as described below. The n^{th} run uses atomic fractional coordinates \mathbf{X}^n of which the i^{th} coordinate is X_i^n where :

$$\begin{aligned} X_i^n &= X_i^{\text{base}} & (i \neq n) \\ X_n^n &= X_n^{\text{base}} + h \end{aligned} \quad (11)$$

and results in forces \mathbf{F}^n .

3. The changes in all atomic forces for each displacement are calculated using :

$$\Delta F_i^n = F_i^n - F_i^{\text{base}}. \quad (12)$$

4. The Hessian matrix A is defined by

$$A_{ni} = \Delta F_i^n / h. \quad (13)$$

5. The Hessian matrix A is decomposed into normalised eigenvectors \mathbf{e}^k each with eigenvalue λ^k .

6. The eigenvectors representing translations (and zero-eigenvalue rotations if there are any) are dropped as described in section 2 *Pfrommer BFGS approach* above. They can be identified as described below. The null movement mode referred to earlier (where individual atomic moves exactly counteract a change in strain) is not present because the Hessian and inverse Hessian do not explicitly include elements relating to strain and stress.
7. All other eigenvalues and eigenvectors are used to build the inverse Hessian H using

$$H_{ij} = \sum_k \frac{e_i^k e_j^k}{\lambda^k} \quad (14)$$

from (3) above. This inverse Hessian is never changed during the phase 2 slab relaxation below.

Phase 2—Slab relaxation

8. The atomic positions within the slab are now relaxed iteratively using

$$\mathbf{X}^{r+1} = \mathbf{X}^r + H\mathbf{F}^r \quad (15)$$

where r is the relaxation iteration number, $\mathbf{X}^0 = \mathbf{X}^{\text{base}}$ and $\mathbf{F}^0 = \mathbf{F}^{\text{base}}$, until the largest residual error is within a factor of 10 of the noise expected in each element.

9. The atomic positions within the slab are now relaxed iteratively using a lower proportion, 0.3, of the calculated move:

$$\mathbf{X}^{r+1} = \mathbf{X}^r + 0.3 \times H\mathbf{F}^r, \quad (16)$$

until either the desired force convergence tolerance has been reached, or the DFT steps show no systematic reduction in residual force. 0.3 is just a factor which works well across later relaxation steps, because it reduces the impact of a large coordinate change solely due to a random, high level of force noise.

10. If the desired force convergence tolerance has not been reached, consider reducing the force noise in each step by one or both of:

- increasing the energy cut off
- applying specific DFT code egg-box removal techniques (discussed below).

and then performing further relaxation steps.

If the desired residual force threshold is not reached in a reasonable number of phase 2 relaxation iterations then the process is now repeated from the first phase 1 step using the atomic configuration with the lowest maximum residual force as the new base configuration.

4.1. Phase 1—Hessian discovery and processing

The Hessian discovery step size h needs to be chosen to be sufficiently large to give a good force signal-to-noise ratio (recommended to be in the range of 30–100) for the largest force change on any atom in each phase 1 Hessian discovery step. It must also be sufficiently small to stay within the linear

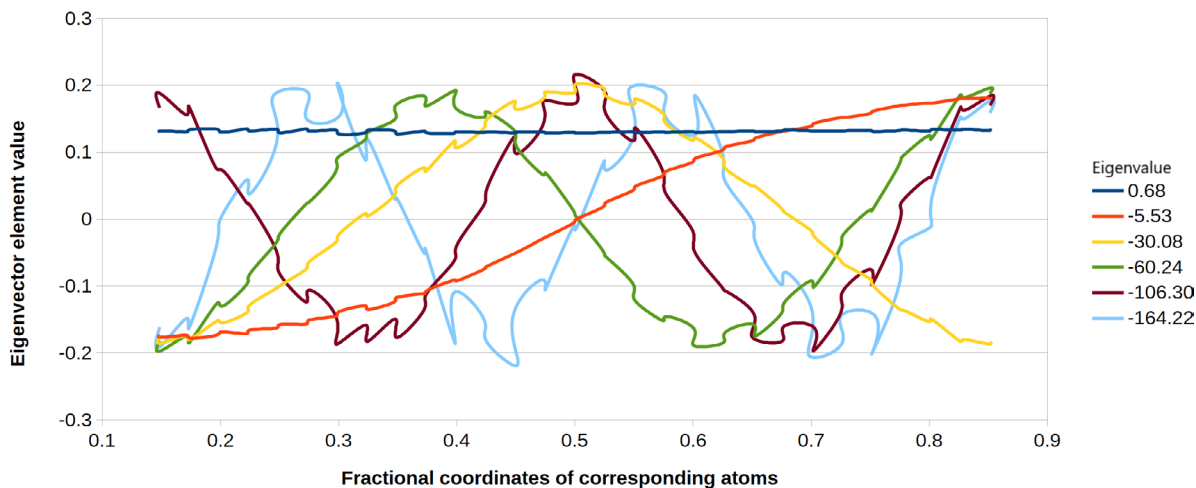


Figure 4. This chart represents the 1D relaxation of a slab with layers $\text{PbTiO}_3 \times 4$, $\text{SrRuO}_3 \times 6$ and $\text{PbTiO}_3 \times 4$ unit cells surrounded by vacuum using the two-phase Hessian approach. The in-plane x and y coordinates of the atomic positions are fixed. For the six eigenvectors of the 1D Hessian with the least negative eigenvalues, the eigenvector coefficient is plotted against the z fractional coordinate of the atom represented by that eigenvector element. The flat eigenvector with eigenvalue 0.68 represents the single 1D translation. All other eigenvectors approximate to cosine waves whose spatial frequencies (proportional to the number of crossings of zero) increase monotonically with more negative eigenvalues. The lines are smoothed using splines with no markers on the points. This produces a clear chart, but also multiple values, where the two atom types in the same plane have similar z fractional coordinates but different eigenvector element values.

displacement/force region around equilibrium, if the initial atomic starting positions permit this. Values for h were typically chosen to result in temporary displacements of 3×10^{-3} Å. The step size, h , was kept constant for all atomic coordinate changes during the Hessian discovery phase.

Using a constant step size h in all phase 1 discovery steps results in a varying force signal-to-noise ratio across discovery steps. A temporary displacement h of certain single atomic coordinates results in a bigger maximum force change on any atom than is produced by the same displacement of other single atomic coordinates. For the second and subsequent times through the two phase process, for each discovery step, h could be varied inversely with the maximum force change produced on any atom for that step the first time through. This would result in similar absolute values for the largest resulting atomic force change for every discovery step, and provide a consistent maximum force signal-to-noise ratio across steps. This enhancement was not implemented.

In the 1D case the single translational eigenvector to be removed from inverse Hessian construction should have an eigenvalue close to zero. It will also have similar values for each eigenvector element.

In the 3D case there will be three orthogonal translational eigenvectors, all with eigenvalues close to zero. The translational eigenvectors' separate x , y and z components should independently have nearly constant elements within that component. Periodic boundary conditions should ensure that rotations within a DFT supercell have non-zero eigenvalues.

Figure 4 shows the Hessian eigenvectors for a 1D triple-layer slab relaxation using the two-phase Hessian approach. The in-plane x and y coordinates of the atomic positions are fixed. In the z dimension the first layer is 4 unit cells thickness of PbTiO_3 , with a second layer of 6 unit cells thickness of SrRuO_3 and a final layer of 4 unit cells thickness of PbTiO_3 . In the z dimension both slab surfaces are surrounded by vacuum.

Each eigenvector coefficient is plotted on the chart y -axis against the z fractional coordinates of the atom corresponding to that eigenvector element. The two different atomic types in each atomic plane have similar z coordinates but different eigenvector element values. The lines are smoothed using splines with no markers on the points. This produces a clear chart, but also multiple values for some fractional coordinates, where multiple atoms in the same plane have similar fractional coordinates but different eigenvector coefficients.

The six eigenvectors of the 1D Hessian with the least negative lowest eigenvalues are displayed. The single translational mode, represented by the flat, dark blue line, has an eigenvalue of 0.68—close to zero as expected. The sinusoidal modes on the chart represent negative Hessian eigenvalues whose eigenvector elements average to zero. Their spatial frequencies increase monotonically as the eigenvalues become more negative.

The two-phase Hessian approach can succeed without incorporating the explicit relationship between stress and strain into the inverse Hessian because the relaxation process is now accurate enough to generate automatically the set of atomic moves required to eliminate linear stress and strain.

If the base structure starts too far from equilibrium then the change in forces used to build the Hessian may not be linear with the additional displacements and the residual force convergence target may not be reached. Further, the noise in the forces in the Hessian discovery steps can magnify particular cross-terms in the Hessian, shifting Hessian eigenvalues, which ought to be negative, closer to zero.

The quality of the discovered Hessian can be evaluated by examination of its eigenvalues and eigenvectors, and the matrix should be symmetric. For eigenvectors which should not be discarded, eigenvalues which are positive or too close to zero are signs that the inverse Hessian quality will not be good enough to relax to a tight residual force tolerance. However, in

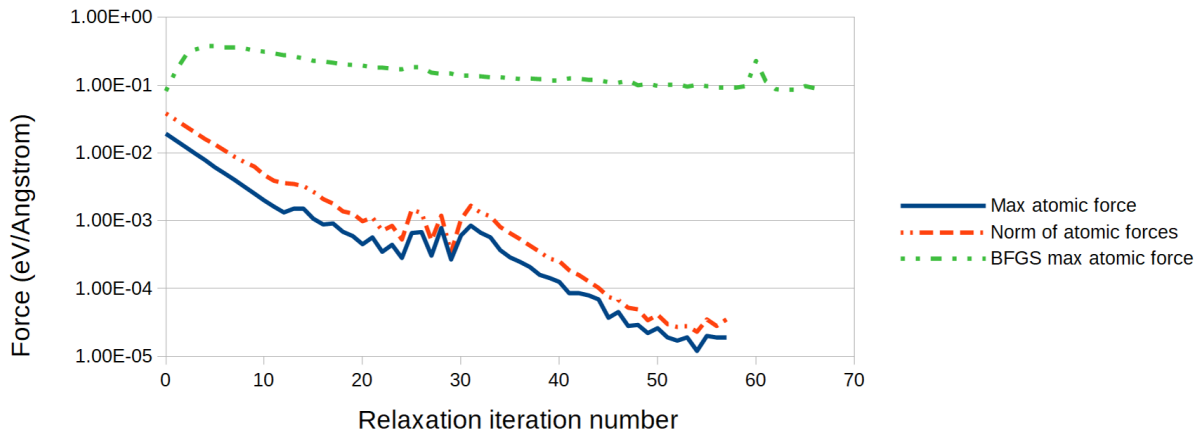


Figure 5. This chart shows two slab relaxations. The red, two dots, three dashes line is the magnitude of the atomic force vector for all atoms, and the blue, solid line is the maximum force on any one atom for a 1D, two-phase Hessian₁ SIESTA relaxation of a $\text{SrTiO}_3 \times 4$ (unit cells)/ $\text{SrRuO}_3 \times 6/\text{SrTiO}_3 \times 4$, 72 atom slab, with an external applied electric field of 1 V \AA^{-1} . The green, two dots, one dash line is for the CASTEP BFGS relaxation of a shorter $\text{SrTiO}_3 \times 3/\text{SrRuO}_3 \times 6/\text{SrTiO}_3 \times 3$, 62 atom slab with no field. Both use a DFT SCF (self-consistent field) energy convergence of 10^{-9} eV/atom . The two-phase Hessian relaxation iteration number shown is for the second, relaxation phase, before which, all 59 phase 1 discovery steps were run. The two-phase Hessian slab converged down to a maximum force on any atom of $1.2 \times 10^{-5} \text{ eV \AA}^{-1}$ after parameters affecting the force noise were changed twice. The number of offsets from each grid point at which forces are calculated and averaged was doubled from 40 to 80 at iteration 15, which did not disrupt the relaxation. The energy cut-off, which also determines the real-space grid spacing, was changed from 1600 eV to 6400 eV at iteration 31, causing an immediate increase in the residual force after which the downward movement resumed. The BFGS relaxation shows much slower convergence, similar to the same slab in figure 1 which was performed with a higher DFT SCF energy convergence of 10^{-7} eV/atom .

1D relaxations, using the phase 1 inverse Hessian in a phase 2 relaxation always lowered the residual forces somewhat, even if the discovered Hessian was not ideal. The partially-relaxed atomic configuration with the lowest residual forces was then selected as the new base atomic configuration and the entire procedure repeated.

Eigensystem decomposition instead of SVD (singular value decomposition) was used in an exploratory manual relaxation of a slab and use continued by default in the automated two-phase Hessian relaxation process. It helped build an intuitive understanding of the quality of the Hessian.

4.2. Phase 2—Slab relaxation

In theory, if the forces are perfectly linear with the displacement from equilibrium, a single application of H to the forces in the base configuration DFT step will completely relax the forces to zero. However, although the complete inverse Hessian H has a lower signal-to-noise ratio than an inverse Hessian generated dynamically using the Pfrommer BFGS algorithm, it is still not perfect. Further, the residual forces to which H is applied also contain noise. Hence multiple iterations are necessary.

Problems were encountered iteratively applying H to low residual forces, just above the convergence tolerance. Hence, from that point, a fraction 0.3 of the calculated move was applied, until the target residual force was reached, or there was no further reduction in residual forces. Using a ball and spring model with Gaussian force noise applied, investigations showed that it is best to allow the initial relaxation steps to use the full move, changing to a fraction of 0.3 only once the maximum residual force on any atom reduces to an order of magnitude larger than the estimate of residual force noise.

4.2.1. Reducing force noise. During the later relaxation steps the residual forces become lower and the relaxation less effective because the force signal-to-noise ratio also reduces. At this point the force signal-to-noise ratio can be improved in various ways.

Increasing the energy cut off will directly reduce the force noise, as it increases the resolution of the DFT real-space grid(s). Increasing the energy cut off part-way through phase 2 relaxation temporarily increases the residual forces because the equilibrium atomic configuration also changes slightly. However, after a few relaxation steps the residual force will be reduced below that before the increase of energy cut off. See figure 5 on page 14.

In DFT codes small changes in nuclear positions with respect to the real-space integration grid cause significant energy changes—the egg-box effect described in Junquera’s slides [6] and in Ruiz-Sessano *et al* 2012 [15]. Apart from increasing the energy cut off, specific DFT codes have specific ways of reducing the impact of the egg-box effect.

In SIESTA, egg-box noise can be reduced by specifying a set of real-space grid fractional offsets with regular spacing at which forces are recalculated. Taking the average of the results across all fractional offsets often reduces the force noise by one or two orders of magnitude, though sometimes this is not effective unless the energy cut off is also increased. CASTEP and other plane wave codes use a real-space fine grid with a resolution which can be altered independently, both of the energy cut off, and of the standard grid scale used for the reciprocal-space grid. Increasing the real-space fine grid resolution reduces egg-box force noise.

SIESTA provides the total of forces along each lattice vector direction for each DFT step—referred to below as the ‘total force discrepancy from zero’. Physically the total should

be zero but in a SIESTA DFT step it often is not. However, when relaxing a centred atomic configuration showing inversion symmetry, the total force discrepancy from zero in each lattice vector direction can be zero or very low. This does not necessarily indicate low force noise, just that most force noise on one atom is not random and is equal and in the opposite direction to the force noise on its inversion-symmetric partner atom, as egg-box effect force noise would be. A similar effect was seen in CASTEP during DFT runs to analyse force noise. Displacing the entire atomic configuration slightly from the centre may expose a higher total force discrepancy from zero.

The techniques above enable most of the processing, including Hessian discovery, to be performed efficiently at higher absolute force noise, but, by using an appropriate discovery step size h , still with large force signal-to-noise ratios. More expensive, lower-noise steps are required only towards the end of the relaxation, optimising overall efficiency.

4.3. Number of DFT steps

The number of DFT job steps for phase 1 Hessian discovery is the number of independent atomic coordinates plus one. For a well formed inverse Hessian the number of phase 2 relaxation steps should be independent of the number of atoms. Typically 30 to 50 relaxation steps sufficed for perovskite slabs of 42–72 atoms.

The number of SCF (DFT self consistent field) iterations per job step (each job step resulting in one set of atomic moves) is greatest for the initial base run. Thereafter, re-use of wave function or density output files as input to subsequent steps reduces the number of SCF iterations. The phase 1 (Hessian discovery) second and subsequent DFT steps take approximately the same time. However, each fractional real-space grid offset contributing towards the average of forces, as described in section 4.2 above, requires a similar time to an SCF iteration.

Although relaxation steps take less time as the phase 2 relaxation proceeds, the constant processing time for the force calculation at multiple fractional offsets starts to dominate the reducing number of SCF iterations per DFT relaxation step. If higher energy cut offs and/or more real-space grid offsets are used to reduce force noise in the later DFT relaxation steps, each subsequent step will be considerably slower than earlier steps. The number of steps cannot readily be compared with those of Pfrommer BFGS (CASTEP) or modified Broyden (SIESTA) as neither of these provided the desired convergence for perovskite slabs without manual intervention.

5. Results

The convergence of the relaxation for an $\text{SrTiO}_3 \times 4$ (unit cells)/ $\text{SrRuO}_3 \times 6/\text{SrTiO}_3 \times 4$, 72 atom slab with external applied field of $1 \text{ V } \text{\AA}^{-1}$; is shown in figure 5. Compared to the results obtained using the initial parameters, parameter changes to reduce the noise in the forces restored the downwards convergence, enabling a reduction in residual forces of a further two orders of magnitude.

Using the two-phase Hessian algorithm the slabs of interest were relaxed to well below the target of $10^{-4} \text{ eV } \text{\AA}^{-1}$ using SIESTA 4.1-b3. Typically, multiple two-phase Hessian runs were required. This compared favourably with those few SIESTA relaxation runs using the modified Broyden method which came close to a higher atomic force convergence target of 2×10^{-4} . But, in those cases, the slab had to be manually (de-)strained multiple times to remove obvious stress before this target could be reached.

A BFGS 1D relaxation of an $\text{SrTiO}_3 \times 3$ (unit cells)/ $\text{SrRuO}_3 \times 6/\text{SrTiO}_3 \times 3$ slab, with no applied field, is also shown on the chart (maximum force on any one atom shown by the green, two dot, one dash line). The convergence of this is very slow. This slab is slightly shorter than those in the SIESTA, two-phase Hessian relaxation, and there is no applied electric field (allowing imposed symmetry). Both of these are reasons why the BFGS relaxation would be expected to be easier and quicker than the two-phase Hessian relaxation.

A comparable SIESTA, modified-Broyden relaxation was not possible, as SIESTA does not allow only one supercell lattice vector to be varied to perform a 1D relaxation.

5.1. 1D simple ball and spring model results

To provide further insight the Pfrommer BFGS and two-phase Hessian relaxation algorithms were tested on a simple 1D ball and spring relaxation model. This model is described in more detail in the supplementary materials (stacks.iop.org/JPhysCM/30/315901/mmedia).

The system studied consisted of a chain of 15 atoms joined by harmonic springs with arbitrary, non-regular, initial spacing and with both random force noise with a Gaussian distribution and egg-box force noise, described in section 4.2.1. The egg-box force noise is sawtooth-shaped, varying periodically with atomic position offset from the nearest grid line of a randomly-positioned grid. The zeroes of the sawtooth occur when an atomic position coincides with a grid line.

For a 15-atom chain, the ball and spring model force convergence reached for each algorithm is shown in table 1.

The ball and spring model was run 100 times each with Gaussian force noise, egg-box noise, or a mixture of the two. Each run consisted of 100 iterations, and the lowest value for the maximum residual force on any individual atom was noted. The higher the fraction of egg-box noise relative to random Gaussian noise, the worse the Pfrommer BFGS algorithm performed relative to the two-phase Hessian algorithm. However, the minimum residual force was highly dependent on the exact resolution and offset of the nominal grid, relative to the expected equilibrium atomic positions. Thus the values in table 1 should be regarded as indicative only.

In the presence of egg-box noise, the Pfrommer BFGS algorithm performed worse. There were also significantly more numerical problems than with the two-phase Hessian approach, caused by breaches of the requirement that the inverse Hessian remains negative semi-definite.

The two-phase Hessian approach gave maximum benefits close to the noise level when only 0.3 of the calculated

Table 1. Comparison of the residual atomic forces, for the Pfrommer BFGS and the two-phase Hessian algorithms, calculated using a 1D ball and spring model of 15 atoms. For each of the force noise settings, each algorithm was run 100 times. Each run consisted of 100 iterations from which the lowest maximum force on any one atom was chosen. The 100 iterations of the two-phase Hessian model do not include the iterations required for the Hessian discovery phase (equal to the number of atoms in the chain plus one). The starting position of atoms was manually adjusted at random. With the addition of significant egg-box noise, the Pfrommer BFGS algorithm performed worse relative to the two-phase Hessian algorithm.

Parameter	Predominant noise type		
	Gaussian	Egg-box	~Equal mixture
Gaussian noise std. dev.	5.0×10^{-7}	0	3.5×10^{-7}
Linear egg-box noise maximum	0	6.2×10^{-7}	4.4×10^{-7}
Combined noise std dev per atom	5.0×10^{-7}	5.0×10^{-7}	5.0×10^{-7}
Average of minimum of BFGS max atomic force	1.9×10^{-6}	6.4×10^{-6}	4.0×10^{-6}
Average of minimum of two-phase Hessian max atomic force	1.3×10^{-6}	2.4×10^{-6}	1.5×10^{-6}

displacement was applied in the following iteration. This technique enabled convergence to lower residual forces than either the Pfrommer BFGS approach or the two-phase Hessian approach when the full calculated displacement was always used.

The two-phase Hessian approach appeared to perform similarly in real DFT runs and in ball and spring model runs. However, the Pfrommer BFGS relaxation performed worse in real DFT runs than in ball and spring model runs, for reasons which we do not understand.

6. Conclusions

The two-phase Hessian approach works well for slabs not successfully relaxed by the modified Broyden or Pfrommer BFGS algorithms. It could also be useful for bulk materials where very low residual forces are more important than run time. The inverse Hessian matrix derived using individual atom moves is constructed from forces with high (30–100) signal-to-noise ratios. In the standard Pfrommer BFGS algorithm the residual forces (i.e. signal), used to dynamically update the inverse Hessian, reduce as the relaxation proceeds, whereas the force noise remains constant. The reduced signal-to-noise ratio degrades dynamic updates applied to the inverse Hessian during the later relaxation steps.

If the two-phase Hessian algorithm is operating in the linear force regime, it is more robust and relaxes to lower residual forces than standard Pfrommer BFGS. If outside the linear force regime, the full two-phase Hessian process needs to be repeated.

The two-phase Hessian procedure allows for increasing the force signal-to-noise ratio towards the end of the relaxation, by

increasing the energy cutoff and/or taking additional measures to counter egg-box effects. This can reduce the residual forces efficiently, incurring the overhead of increased calculation only when necessary. In principle this could also be implemented in the Pfrommer BFGS algorithm, but care would be necessary to avoid updating the dynamic inverse Hessian for the step during which a higher energy cut off was first used, as the forces would change purely because of a new equilibrium atomic configuration caused by the higher energy cut off. This would cause a bad inverse Hessian update for that step. Similar considerations apply to modified Broyden.

The supplementary materials contain implementation details for the two-phase Hessian process and further details of the 1D ball and spring model.

Acknowledgments

We are grateful to the UK Materials and Molecular Modelling Hub for computational resources, which is partially funded by EPSRC (EP/P020194/1).

We are also grateful to Dr Phil Hasnip and Prof Matt Probert of the University of York for help with CASTEP and to Dr Nick Bristowe of the University of Kent for help with SIESTA.

ORCID iDs

P A G Davies  <https://orcid.org/0000-0003-4141-419X>

W M C Foulkes  <https://orcid.org/0000-0001-8359-1122>

References

- [1] Artacho E *et al* 2017 User's Guide SIESTA 4.1-b3 <https://launchpad.net/siesta>
- [2] Broyden C G 1965 A class of methods for solving nonlinear simultaneous equations *Math. Comput.* **19** 577–93
- [3] Clark S J *et al* 2005 First principles methods using CASTEP *Z. Kristallogr.* **220** 567–70
- [4] Dharmawardhana C C 2015 Structure and mechanical properties of cement and intermetallic compounds via *ab initio* simulations *PhD Thesis* University of Missouri, Kansas City
- [5] Johnson D D 1988 Modified Broyden's method for accelerating convergence in self-consistent calculations *Phys. Rev. B* **38** 12807–13
- [6] Junquera J 2010 Course notes: The eggbox effect: converging the mesh cutoff. (Presentation) http://personales.unican.es/junqueraj/JavierJunquera_files/Metodos/Convergence/Eggbox-MgO/Exercise-eggbox-MgO.pdf, <http://slideplayer.com/slide/8542227/>
- [7] Knuth F *et al* 2015 All-electron formalism for total energy strain derivatives and stress tensor components for numeric atom-centered orbitals *Comput. Phys. Commun.* **190** 33–50
- [8] Liu Y *et al* 2009 Negative pressure induced ferroelectric phase transition in rutile TiO₂ *J. Phys.: Condens. Matter* **21** 275901
- [9] Nocedal J and Wright S 2006 *Numerical Optimization* (New York: Springer)
- [10] Parliński K 2005 First-principles calculations of vibrational and thermodynamical properties of solids *Materials Science-Poland* **23** 357–63

- [11] Pfrommer B G *et al* 1997 Relaxation of crystals with the quasi-Newton method *J. Comput. Phys.* **131** 233–40
- [12] Piskunov S *et al* 2004 Bulk properties and electronic structure of SrTiO₃, BaTiO₃, PbTiO₃ perovskites: an *ab initio* HF/DFT study *Comput. Mater. Sci.* **29** 165–78
- [13] Press W H *et al* 2007 *Numerical Recipes: the Art of Scientific Computing* 3rd edn (Cambridge: Cambridge University Press)
- [14] QuantumWise 2018 Electron transport calculations with electron–phonon coupling included via the special thermal displacement method—STD-Landauer https://docs.quantumwise.com/casestudies/std_transport/std_transport.html (Accessed: 24 May 2018)
- [15] Ruiz-Serrano \tilde{A} , Hine N D and Skylaris C-K 2012 Pulay forces from localized orbitals optimized *in situ* using a psinc basis set *J. Chem. Phys.* **136** 234101
- [16] Shah S H *et al* 2008 First principles study of three-component SrTiO₃/BaTiO₃/PbTiO₃ ferroelectric superlattices *J. Mater. Sci.* **43** 3750–60
- [17] Srivastava G P 1984 Broyden’s method for self-consistent field convergence acceleration *J. Phys. A: Math. Gen.* **17** L317
- [18] Vanderbilt D and Louie S G 1984 Total energies of diamond (1 1 1) surface reconstructions by a linear combination of atomic orbitals method *Phys. Rev. B* **30** 6118–30